

# Integrated Flexible, Waterproof, Transparent, and Self-Powered Tactile Sensing Panel

Xu-Zhou Jiang,<sup>‡,§</sup> Yi-Jing Sun,<sup>§</sup> Zhiyong Fan,<sup>\*,‡</sup> and Tong-Yi Zhang<sup>\*,†</sup>

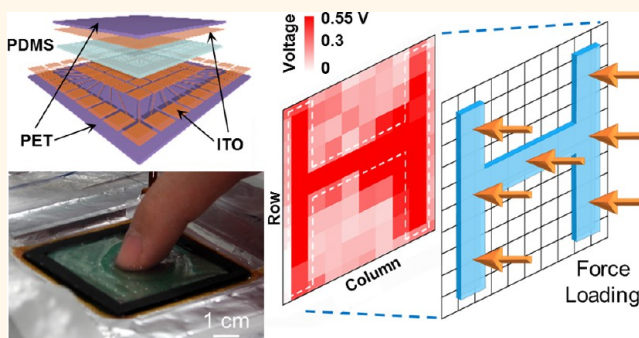
<sup>†</sup>Shanghai University Materials Genome Institute and Shanghai Materials Genome Institute, Shanghai University, 99 Shangda Road, Shanghai 200444, China

<sup>‡</sup>Department of Electronic and Computer Engineering and <sup>§</sup>Department of Mechanical and Aerospace Engineering, The Hong Kong University of Scientific and Technology, Clear Water Bay, Kowloon, Hong Kong SAR, P. R. China

## S Supporting Information

**ABSTRACT:** Portable and wearable electronic devices are human-centered devices; therefore, many unique attributes are highly desirable, such as flexibility, being self-powered, and waterproof. These properties render devices excellent adaptivity in harsh operation environments. In this work, we report an integrated triboelectric tactile sensor array with flexible, transparent, self-powered, and waterproof features. Each tactile sensor is a surface nano/microtexture enhanced triboelectric nanogenerator. The sensor array can serve as a touch panel for electronic devices. Owing to a unique design of a built-in triboelectric contact pair and an electrical shielding layer, an individual pixel of the fabricated tactile sensor array can generate an open circuit voltage up to 1.613 V and a short circuit current density of 47.308 mA/m<sup>2</sup> under 612.5 kPa. The tactile sensors can produce stable voltage signals regardless of the materials of the touching objects, and work stably both in ambient and aqueous environments. To examine the touch panel function of a sensor array, a matrix of 10 × 10 individually addressable 4 mm × 4 mm triboelectric sensors has been integrated into a thin, transparent, and flexible film, and the 2-D touch mapping has been successfully demonstrated. The unique triboelectric tactile sensor array reported here is robust and highly versatile, and it may find broad applications in display, wearable electronics, artificial skins, Internet of Things (IoT), etc.

**KEYWORDS:** triboelectric effect, waterproof, self-powered device, tactile sensor, touch panel



One of the most popular and important interfacing devices for human-machine interaction is the touch panel device, especially for personal electronics. Currently, the mainstream touch panels are based on capacitive sensing technology. As a passive device, a capacitive sensor consumes power during operation. In addition, it is primarily a two-dimensional input device which cannot directly measure the touch force/pressure. Another major drawback of capacitive sensors that are being widely used on cell phone displays is that water droplets on sensors cause false touch signals. In a mainstream mutual capacitive touch sensor, transmit and receive electrodes arranged as an orthogonalized matrix are isolated by a dielectric layer. In each intersection node, one transmit electrode and one receive electrode form an inherent capacitor. When a conductive object, i.e., a human finger, approaches this node, the coupling capacitor from the finger in parallel with the inherent capacitor increases the capacitance between the two electrodes. By measuring this capacitance change, the touch position can be determined. However, water droplets falling on a capacitive touch panel in daily life are also

conductive thus can replace human finger touch input in the measurement circuit to cause false signals and malfunctions of touch sensing. These existing issues limit the applications of capacitive sensors. Recently, wearable and portable electronics have attracted enormous attention worldwide.<sup>1–8</sup> For these devices, the operation environment of touch panel devices is usually complex, and thus unique attributes such as being flexible and waterproof as well as self-powered are highly desirable. Recent studies on triboelectricity revealed that, based on the contact electrification effect when human skin touches against the material of device surface, coupled with the electrostatic charge induction, flexible triboelectric tactile sensors can directly convert mechanical energy into electron flow without any external power supply, and thus they are naturally self-powered devices.<sup>9–12</sup> It has been demonstrated

Received: May 8, 2016

Accepted: June 22, 2016

Published: June 22, 2016

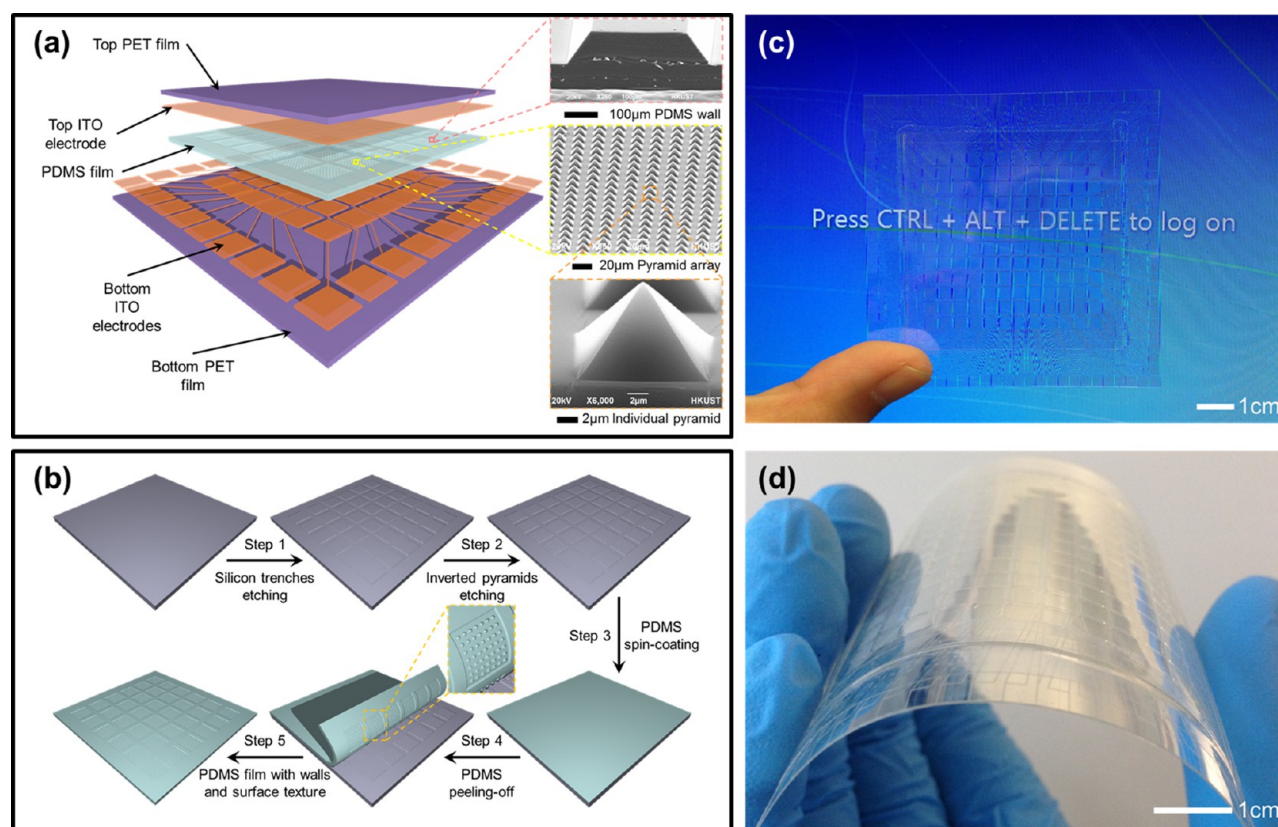


**Figure 1.** (a) Schematic illustration of the integrated triboelectric tactile sensor array. Insets: SEM images of the PDMS wall and PDMS pyramids. (b) Schematics of the fabrication process flow of the PDMS film with wall network and surface textures. (c) Photograph of the as-fabricated device on a commercial desktop display. (d) Photograph of the bent device.

that triboelectric devices usually deliver higher voltage output than piezoelectric touch sensor devices with a given pressure input.<sup>7,13,14</sup> These attractive features make triboelectric devices highly promising for applications in display, wearable electronics, artificial skins, implantable devices, and IoT, as both tactile sensors<sup>9–12</sup> and energy scavengers.<sup>15–20</sup>

Meanwhile, it is worth pointing out that most of the reported flexible triboelectric tactile sensors are open to the normal surroundings and use human skin as one contact material for triboelectric charge generation.<sup>9–12,21</sup> Therefore, the reported sensor devices still cannot be used in the environments with water presence, which can also be one contact material instead of human skin,<sup>17,20,22,23</sup> and the sensor output can be easily affected by local humidity. Moreover, not only water but also any other object with a different material, like a glove, a touch pen, and so on, can replace human skin in the reported sensors to generate triboelectric charges. The quantity of the generated charges depends on the position of the material in the triboelectric series, which further determines the electrical output voltage under certain mechanical loading conditions. These are particularly constraints for many applications such as wearable devices for sports, artificial skins, *etc.* In this work, we present an integrated triboelectric tactile sensor array, which is a device combining characteristics of being self-powered, highly flexible, transparent, and waterproof. The sensor array has 100 addressable pixels, which has so far the largest pixel number in the past reports on triboelectric force sensor arrays.<sup>9,11,12</sup> For each individual sensor pixel, transparent indium tin oxide (ITO) films are used as both top and bottom electrodes, and thus the entire device has good transparency. In this device

configuration, the contact area between the PDMS micro-pyramids and the top ITO electrode is determined by the contact force; therefore, the sensor output voltage is proportional to the contact pressure and the touch pressure can be precisely measured. In addition, the global top ITO electrode is grounded to shield the device from external electrical interference, including the parasitic triboelectric effect between the surface of the device and the touching objects, for example, a human finger or water droplet. Therefore, the sensors can reliably respond to touch with any object, and they are functional even in water. To demonstrate a concept-proof self-powered touch panel, a matrix of  $10 \times 10$  individually addressable triboelectric nanogenerators/sensors has been fabricated and examined. It was found that the peak voltage of a single pixel can reach up to  $1.938 \pm 0.068$  V, which can be easily detected and processed by the external measurement circuit. A dynamic response test showed that the sensor devices have fast response speed. In addition, the touch panel demonstrated the capability to respond to multitouch and reconstruct patterned touch signal. Overall, the work reported here is a significant step toward the practical self-powered tactile sensors applicable in harsh environments which may find broad applications in wearable electronics, artificial skins, implantable devices, IoT, *etc.*

## RESULTS AND DISCUSSION

As schematically shown in Figure 1a, the waterproof tactile sensor array consists of five layers of materials from top to bottom, including a polyester (PET) protective layer, a global ITO layer, a PDMS layer, an addressable ITO electrodes layer,

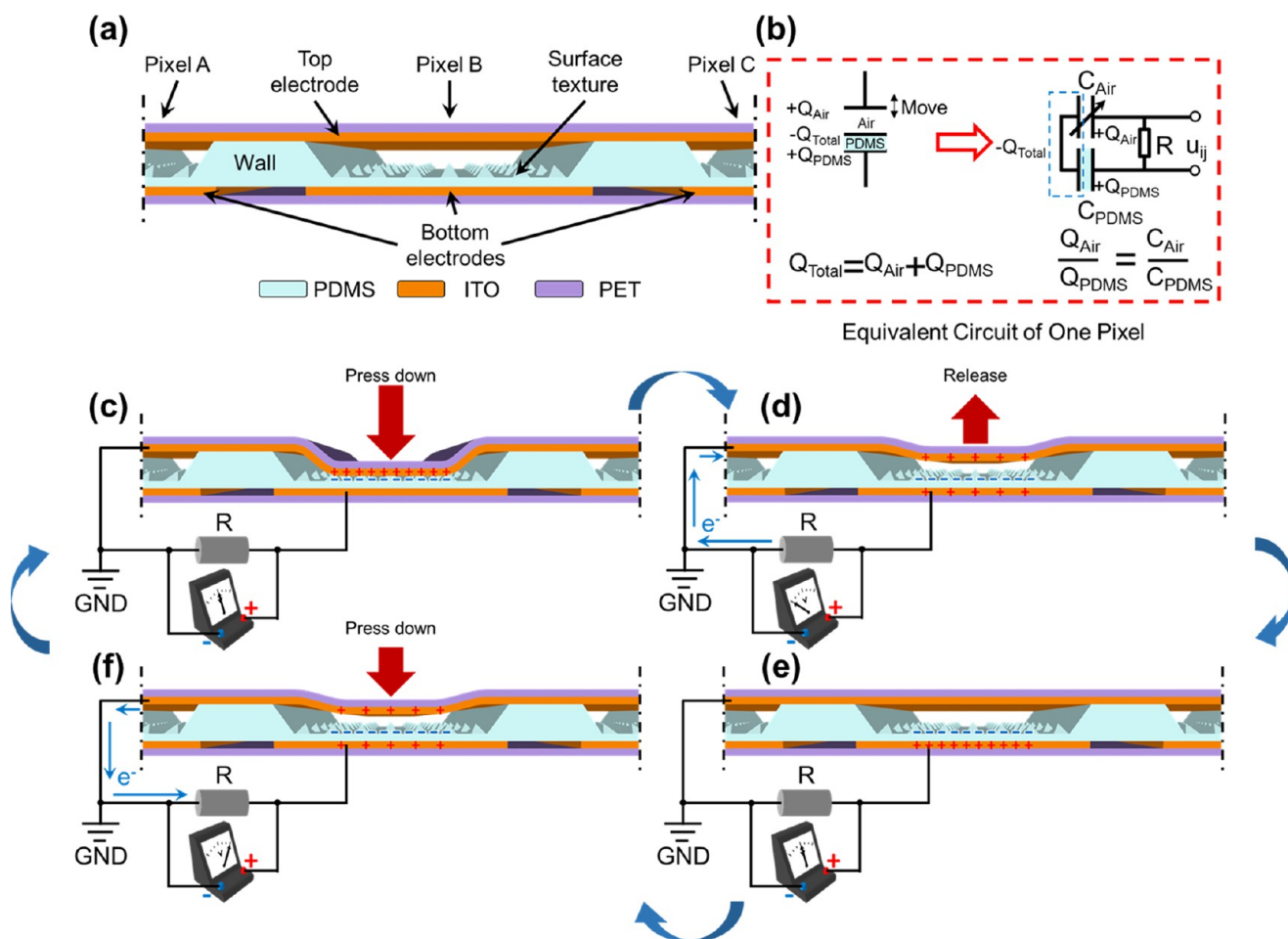


**Figure 2.** Schematic drawings of the working principle of one pixel in the integrated triboelectric tactile sensor array. (a) Detailed cross-sectional structure of one pixel (Pixel B) with its neighborhoods (Pixels A and C). (b) Equivalent circuit of one pixel. (c) Top ITO electrode and PDMS surface with pyramids fully contact driven by an external pressure, generating positive charges on the ITO side and negative charges on the PDMS side by a triboelectric effect. (d) Due to the withdrawal of the external pressure, separation of the two surfaces pumps electrons into the bottom ITO electrode from the top ITO electrode to balance the potential differences of the two capacitors in parallel. (e) The top ITO electrodes rebound to the initial position, and new electrostatic balance is reached by the redistribution of the triboelectric charges. (f) As the external pressure is applied again, electrons are driven back to the top ITO electrode by the change of  $C_{Air}$ .

and a supportive PET layer. In an actual tactile panel device, there are  $10 \times 10$  arrays of PDMS micropyramids separated by PDMS side walls. The PDMS side walls and pyramids were fabricated with a Si mold with the inverted corresponding structures. The schematic fabrication process flow of the Si mold and the PDMS film is shown in Figure 1b. Briefly, the Si mold was fabricated by photolithography and two-step anisotropic wet etching to form a trench network and inverted pyramids. The PDMS film was cured and peeled off carefully after being cast on the Si mold. The process details can be found in the Experimental Section. The insets in Figure 1a are the scanning electron microscopy (SEM) images of the cross-section of a PDMS wall, a pyramid array, and an individual pyramid from top to bottom. The  $90 \mu\text{m}$  tall and  $400 \mu\text{m}$  wide PDMS walls and  $10 \mu\text{m} \times 10 \mu\text{m}$  PDMS pyramids are supported by a  $65 \mu\text{m}$  thick flat PDMS film. Note that it has been discovered that a pyramid shape is preferred<sup>24–27</sup> and  $10 \mu\text{m} \times 10 \mu\text{m}$  size is the optimized geometry.<sup>5</sup> Therefore, we have adopted this geometrical design guideline in our work. In this case, each PDMS pyramid array occupies  $4 \text{ mm} \times 4 \text{ mm}$  area, and it has  $160 \times 160$  micropyramids surrounded by PDMS walls. As shown in Figure 1a, the bottom ITO layer

( $500 \text{ nm}$  thick) coated on the PET film ( $127 \mu\text{m}$  thick) was pixelated by using laser cutting, and the bottom electrode of each pixel is electrical connected to a corresponding ITO pad outside the coverage of the PDMS film for wire bonding to a specifically designed printable circuit board (PCB) for signal acquisition and consequent data processing. By carefully aligning and stacking all the layers together, the waterproof tactile sensor array was assembled as a flexible and transparent device with an overall thickness of less than  $500 \mu\text{m}$ . Photographs in Figure 1c and 1d demonstrate the attractive transparency and flexibility of the fabricated device.

A more detailed cross-sectional schematic drawing of one single pixel (Pixel B) with its two neighboring pixels (Pixels A and C) is illustrated in Figure 2a. Supported by side walls, the designed built-in triboelectric pair, i.e., the top ITO electrode and the PDMS film, is separated by air. Unlike the global top ITO layer, the bottom ITO layer is pixelated, and each individual pixel is addressable. By assuming the air gap between the top surface of the PDMS layer and the top ITO electrode contributes to an adjustable air capacitor ( $C_{Air}$ ) in each pixel and the PDMS film within one pixel as a constant capacitor ( $C_{PDMS}$ ), these two capacitors are sharing one electrode (the

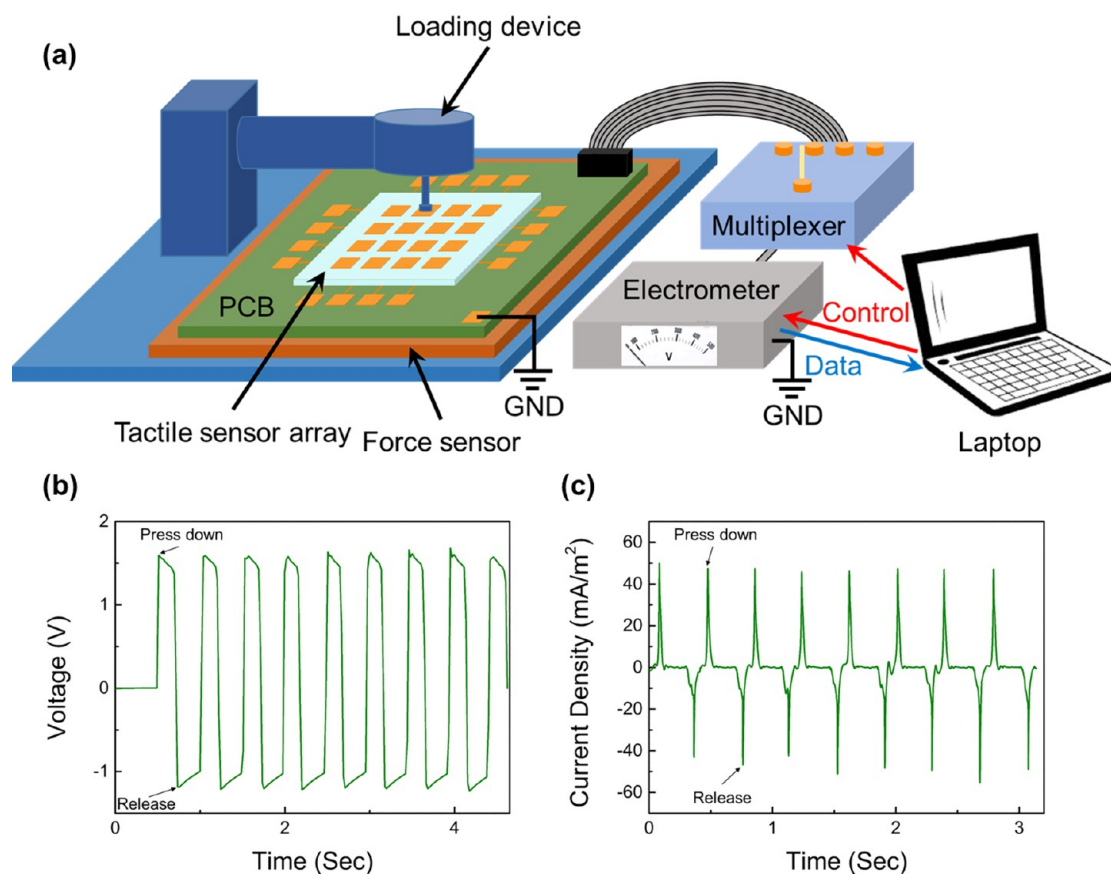


**Figure 3.** (a) Schematic illustration of the experimental setup. (b) Measured open circuit voltage of one pixel in the sensor array up to  $1.613 \pm 0.036$  V. (c) Measured short circuit current density of one pixel in the matrix up to  $47.308 \pm 1.141$  mA/m<sup>2</sup>.

top surface of the PDMS film) and connected in parallel, as the equivalent circuit shown in Figure 2b. The working principle of one pixel inside this tactile sensor array is schematically described in Figure 2c to f. When the Pixel B is pressed down by an external load, for example, a finger tapping, the top ITO layer and PDMS film come into contact within this pixel, while the neighboring pixels remain undeformed due to the mechanical support of the side walls, as shown in Figure 2c. Due to the fact that PDMS is more triboelectrically negative than ITO, electrons are transferred from the ITO surface to the PDMS surface during contact,<sup>28</sup> leading to a positively charged ITO layer and a negatively charged PDMS layer. These charges generated by the triboelectric effect are the total charges stored in the two capacitors of one single pixel and considered as a constant during one loading cycle. When ITO and PDMS are in physical contact, the two surfaces can be considered as infinitely close, resulting in an infinite  $C_{\text{Air}}$  to store all the charges, zero potential difference across both capacitors, and no current flow delivered to the external circuit. As soon as the external pressure is removed, the two surfaces are separated by the restoring force of the PDMS walls leading to a dramatic reduction of  $C_{\text{Air}}$  and the potential difference across  $C_{\text{Air}}$  increases significantly, meanwhile the potential difference across  $C_{\text{PDMS}}$  still remains unchanged. To balance the potential difference of the two capacitors in parallel, electrons flow from the ground to the top ITO electrode to neutralize the positive charges and reduce the potential difference across  $C_{\text{Air}}$ , and electrons are expelled from the bottom ITO electrode to increase the potential difference across  $C_{\text{PDMS}}$ . The distribution of the total charges is determined by the value of the two

capacitors in parallel, as shown in Figure 2b. Therefore, the net consequence of this process is that negative charges are generated and kept on PDMS pyramids, and there is a surge of external current flow from the top ITO to the bottom ITO electrode, as shown in Figure 2d. In the end of the process, as shown in Figure 2e, there are almost no net positive charges on the top ITO electrode. In the next loading cycle, when the top ITO is approaching PDMS pyramids, as shown in Figure 2f, positive charges are induced in the top ITO and electrons flow out from the top ITO, accompanied by electrons flowing into the bottom ITO electrode thus the external current flows back from the bottom ITO to the top ITO.

On the other hand, the untouched pixels, i.e. Pixels A and C in Figure 2a, remain undeformed in the above-mentioned cycle and output zero signals. Moreover, the grounded top ITO electrode ensures that all the charges generated by interference sources, including the triboelectric effect between the device surface and the touching objects, residual charges on the touching objects, environmental EMI, etc., can be dumped into the ground, while only the charges produced by the activated triboelectric contact, i.e., ITO against PDMS, can flow into the measurement unit. This feature makes sure that the electrical outputs are reliable and insensitive to the surroundings and the materials of the touching objects thus are only sensitive to mechanical loadings. This is closer to an ideal tactile sensor, for example, human skin.

In order to systematically characterize the sensor performance, a homemade testing system has been built up as schematically shown in Figure 3a. Briefly, the loading tip geometry is a 4 mm × 4 mm square plate; the applied force was

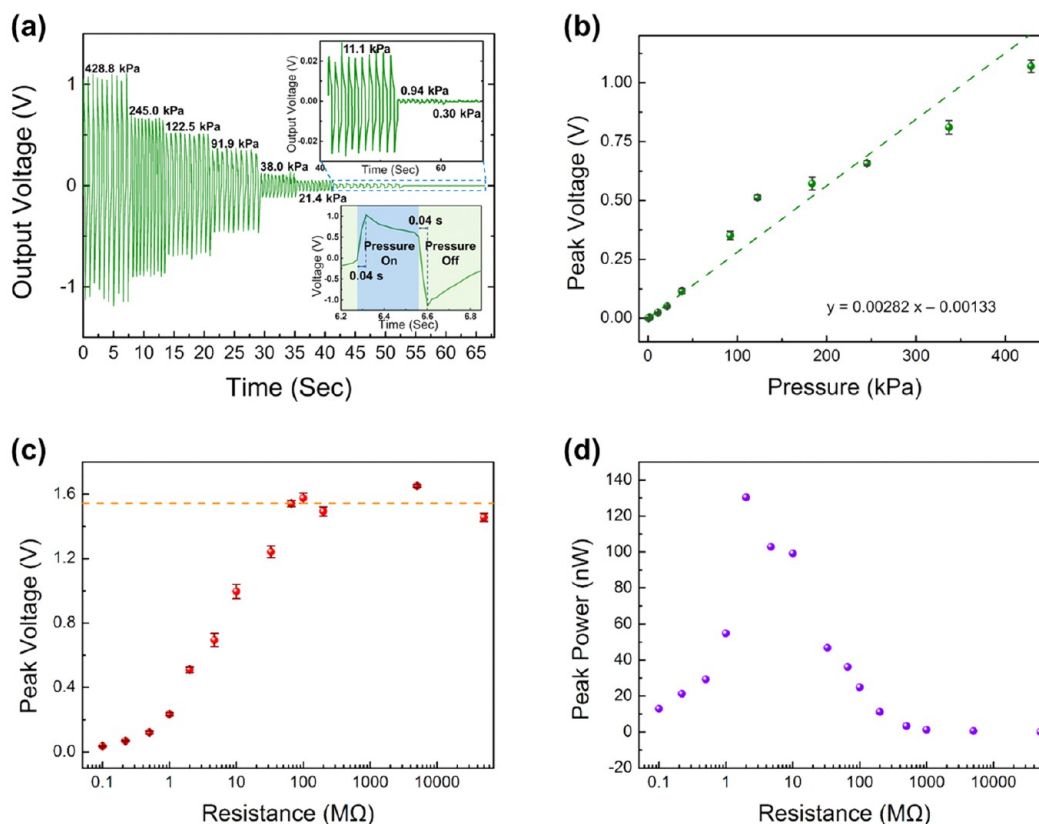


**Figure 4.** (a) Measured voltage of one typical pixel in the matrix under different pressures. Insets: Detailed voltage curves of low pressures and the magnified output curve in one cycle under 428.8 kPa pressure loading. The response time is around 0.04 s in both pressure on and pressure off processes. (b) Output voltage as a function of the external pressure. The green dashed line represents the linear fitting function. (c) Measured voltage of one device in the array with different external resistances. The orange dashed line indicates a saturated value of 1.54 V with large resistances. (d) Calculated power of one pixel in the matrix with different external resistances.

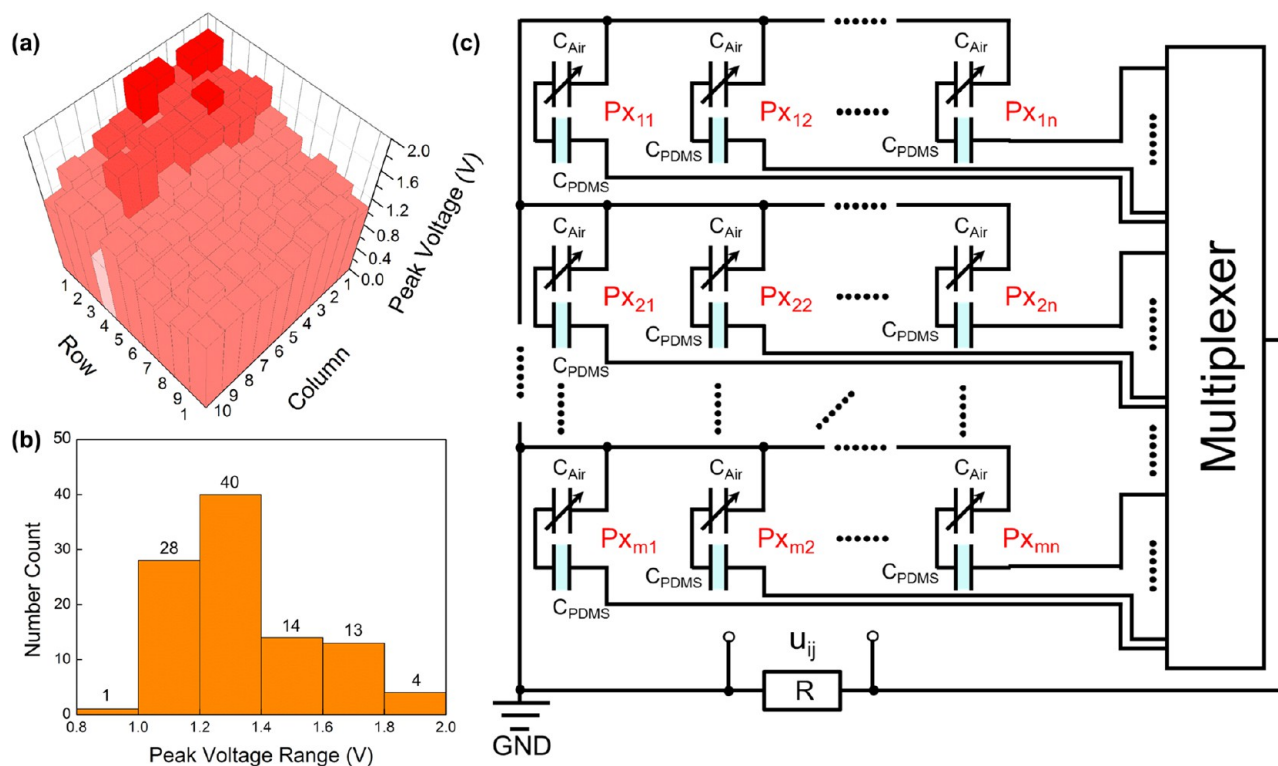
recorded by a force sensor underneath the tactile sensor array, and the electrical outputs were delivered through a customized PCB, a multiplexer, and an electrometer, sequentially, and eventually recorded by a computer. The multiplexer was controlled by the computer to either address a constant channel for single pixel performance characterization or scan up to 100 channels for 2-D touch mapping. Figure 3b presents the typical measured open circuit voltages of one selected pixel with a pressure of 612.5 kPa and loading rate of 10 mm/s, where the magnitude of voltage peaks was  $1.613 \pm 0.036$  V. The corresponding short circuit current density with the same loading pressure reached  $47.308 \pm 1.141$  mA/m<sup>2</sup>, as illustrated in Figure 3c.

Figure 4a presents the output voltage peaks of one single pixel by applying alternating loading pressure with different magnitudes with an external resistance of 1 G $\Omega$ , revealing an increase of output voltage with an increase of loading pressure. The upper inset of Figure 4a shows that as small as 0.30 kPa pressure can be measured by the current circuit. The lower inset of Figure 4a is the magnified output curve in one cycle under 428.8 kPa pressure loading. The response time is around 0.04 s in both pressure on and pressure off processes. Note that this measurement may have overestimated the response time as the input mechanical stimulation may not be an ideal square waveform. Furthermore, as depicted in Figure 4b, the output voltage peak height of this triboelectric tactile sensor exhibits a close to linear relationship with the magnitudes of the applied loading by fitting the experiment data, and the sensitivity of the

pressure is around  $2.82 \pm 0.187$  V/MPa. This property suggests that the triboelectric tactile sensor array can detect not only the locations of touches but also their magnitudes.

In experiments, we discovered that the electrical outputs of the fabricated triboelectric tactile sensors can also be affected by the external resistance, as shown in Figure 4c. The peak voltage across the resistor connected between the bottom electrode and ground generated by a mechanical loading of 612.5 kPa and a loading rate of 10 mm/s monotonically increases up to 1.54 V when the external resistance is less than 66 M $\Omega$ , and it remains almost as a constant when the resistance is greater than 66 M $\Omega$ . Figure 4d demonstrates the peak power obtained with different external resistances as the products of the peak voltage and the corresponding current. The maximum power output occurs at 2 M $\Omega$  as the optimized external circuit condition for energy conversion. However, as the peak voltage is the more important parameter in our measurement, in most experiments 1 G $\Omega$  external resistance was used.

Although undergoing the same fabrication process, the performance of individual pixel may have variations. To evaluate this variation, the peak voltage values of pixels were measured with the same testing conditions, namely, 612.5 kPa pressure with a loading rate of 10 mm/s and 1 G $\Omega$  external resistance, and plotted into a 3-D voltage map, as shown in Figure 5a. After repeating 10 loading cycles, the average peak voltage for all 100 pixels in the triboelectric tactile sensor array is  $1.341 \pm 0.217$  V with a maximum value of  $1.938 \pm 0.068$  V and a minimum value of  $0.884 \pm 0.073$  V. Figure 5b shows the



**Figure 5.** (a) Measured output voltage distribution of all 100 devices in the matrix. The average value is  $1.341 \pm 0.217$  V. (b) The statistical sorting of the voltage outputs of all 100 devices in the array with different ranges. (c) Circuit schematic of the sensor matrix to address individual pixels by a multiplexer.

histogram of the peak voltage, where 40% are in the range from 1.2 to 1.4 V and 82% are from 1.0 to 1.6 V. This reasonably good performance variation data was recorded and utilized in 2-D touch scanning test as a calibration matrix to normalize the outputs of different pixels.

According to the equivalent circuit of one single pixel in Figure 2b, the 2-D scanning circuit is schematically illustrated in Figure 5c to address individual pixels by a multiplexer. Any charge flow of an individual pixel resulting from the change of  $C_{Air}$  by mechanical loading can be detected and recorded as a voltage peak, when this pixel is connected with the measurement unit by the multiplexer. After going through all the pixels, a customized software can acquire all the voltage output data from each pixel and generate a 2-D map to indicate the locations and pressures of the mechanical touches.

To demonstrate the mapping functionality of the integrated tactile sensor array, 2-D scanning tests of both single pixel touching and multiple pixels simultaneous touching were conducted. As shown in Figure 6a, the result of single touching test obviously indicates the location of the individual pressed pixel, i.e., row 6 and column 6; and the peak voltage from the touched pixel is 1.034 V, whose corresponding calculated pressure is 367.012 kPa according to the linear fitting equation obtained from Figure 4b which is close to the measured pressure (428.750 kPa). It is worth noting that the pixels at row 6 and column 5 and row 6 and column 7 also show 0.321 and 0.238 V outputs, respectively, even though they were not depressed. This is because interpixel resistance is not infinite and few current leakages always exist among pixels.

The demonstration for multiple pixel simultaneous touching is shown in Figure 6c. An H-shape PDMS mold was fabricated and placed on the triboelectric tactile sensor array surface, as

shown in Figure 6b, to transfer a patterned loading from a specialized loading head to the triboelectric tactile sensor array. Figure 6c shows the 2-D map of the output peak voltage. By setting 0.55 V as the cutting off value in the 2-D map, the H-shape pattern can be clearly recognized from the darkest red color pixels. The average peak voltage of the touched pixels is  $0.624 \pm 0.177$  V, corresponding to a calculated pressure of  $221.748 \pm 63.238$  kPa, while the average peak voltage of the unloaded pixels is  $0.174 \pm 0.075$  V. More details of this demonstration with several real-time loading and unloading cycles can be seen from supplementary movie 1 which confirms the reproducibility and reliability of the multiple pixel touching detection.

One of the key advantages of our tactile sensor design is that the triboelectric material pair is encapsulated so that the device can be operated in a harsh environment including in water. To demonstrate the device waterproof functionality, a homemade water reservoir was mounted on the sensor array to ensure the entire sensor array is covered by water, as illustrated in Figure 7a. The time-resolved voltage response is plotted in Figure 7b resulting from the touches in water by a bare finger, and its corresponding control group sensing without water is shown in Figure 7c. The higher peaks are from hard press actions ( $210.455 \pm 16.399$  kPa in air and  $248.430 \pm 8.268$  kPa in water), while the lower peaks are generated by the gentle press of a human finger ( $26.583 \pm 4.856$  kPa in air and  $54.880 \pm 7.218$  kPa in water). In both plotted figures, the average values of lower peaks are  $0.0486 \pm 0.0132$  V in air and  $0.114 \pm 0.048$  V in water, and the average values of higher peaks are  $0.386 \pm 0.081$  V in air and  $0.474 \pm 0.053$  V in water, to prove that the aqueous working environment cannot influence the performance of this integrated triboelectric tactile sensor array. More

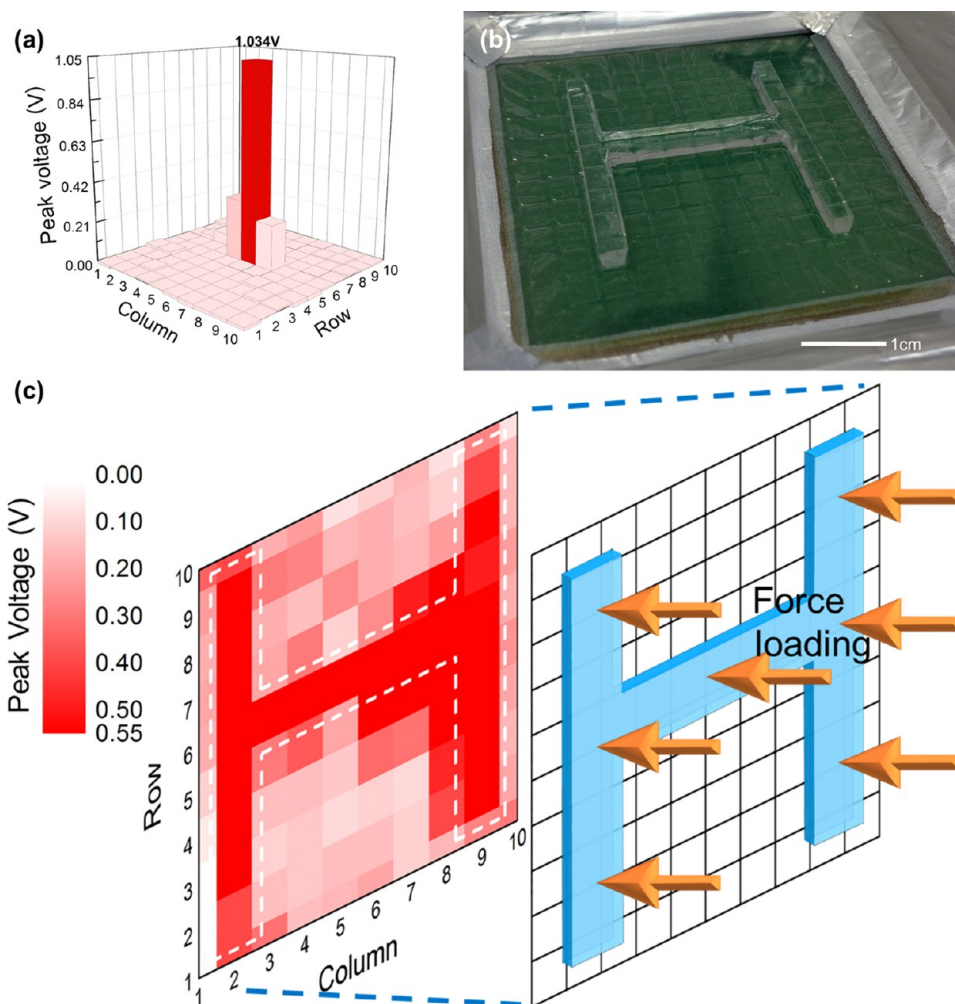


**Figure 6.** (a) The mapping figures of a single touch in 3D view. (b) An H-shape PDMS mold on the sensor array. (c) Top view of the mapping result of multiple touches with an H-shape PDMS mold. The average voltage peak of the touched pixels is  $0.624 \pm 0.177$  V, corresponding to a calculated pressure of  $823.114 \pm 234.292$  kPa, while the average voltage peak of the unloaded pixels is  $0.174 \pm 0.075$  V.

details of this demonstrate are illustrated in [supplementary movies 2 and 3](#) in real-time.

Besides the waterproof test, the reliability of this fabricated triboelectric tactile sensor array touched by objects with different materials was examined with three different common objects of a piece of aluminum foil, a lab glove, and a fingertip, representing metals, polymers, and human skin, as shown in the inset of [Figure 7d](#). The result of this demonstration exhibits that the peak voltages generated from different touching materials are around 0.6 V with similar loading pressures, and they are  $0.548 \pm 0.068$  V,  $0.573 \pm 0.052$  V, and  $0.703 \pm 0.063$  V, touched by the aluminum foil, the glove, and the human skin, respectively, under loading pressures of  $265.213 \pm 10.169$  kPa,  $280.280 \pm 7.295$  kPa, and  $326.218 \pm 11.468$  kPa, as shown in [Figure 7d](#), because the electrical outputs were only produced by the built-in triboelectric contact, i.e., PDMS against ITO inside the device. This demonstration experimentally proves that this triboelectric tactile sensor array is independent of the different materials of the touching objects, which is one side of the triboelectric pair in pervious integrated triboelectric tactile sensor arrays. More details of this demonstrate are shown in [supplementary movie 4](#).

## CONCLUSION

In summary, we have demonstrated a unique flexible, transparent, and waterproof triboelectric tactile sensor array with  $10 \times 10$  pixels, based on a built-in triboelectric pair of ITO and PDMS micropylamids. By converting the mechanical energy from the touching motions, one selected pixel of this sensor array can produce an open circuit voltage up to  $1.613 \pm 0.036$  V and a short circuit density of  $47.308 \pm 1.141$  mA/m<sup>2</sup>. The pressure sensitivity of the selected pixel is about  $2.82 \pm 0.187$  V/MPa, and the pressure as low as 0.30 kPa can be detected. The sensor array exhibits a consistent performance distribution across the whole device with an average voltage output of  $1.341 \pm 0.217$  V loaded by 612.5 kPa pressure. A testing system controlled by customized software was built to characterize the capability of the sensor array for mapping the mechanical touch locations and the magnitudes, for both single pixel touch and multiple pixels touch simultaneously. The sensor array is waterproof, operated independently of the materials of touching objects, and sensitive only to loading pressure. This is a highly desirable feature for an ideal tactile sensor, such as human skin. Combining with other attractive properties, including excellent transparency and flexibility, the tactile sensor array demonstrated in this work has a high

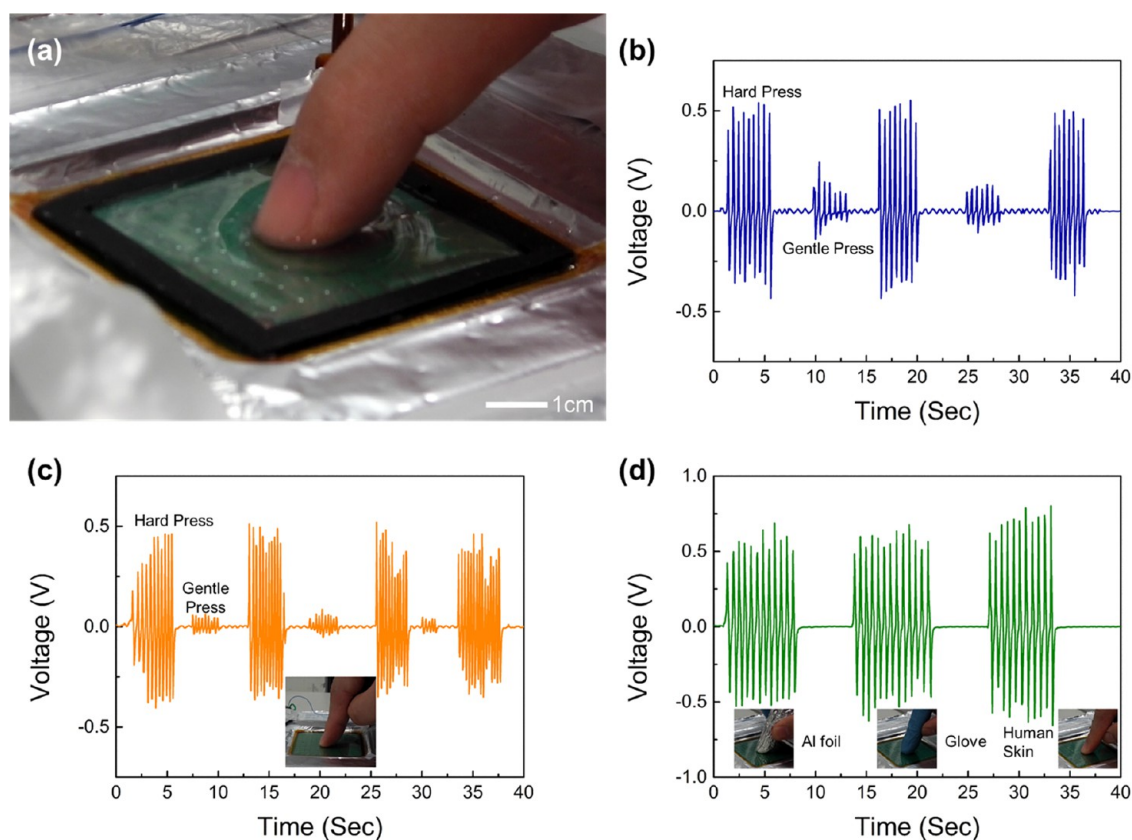


**Figure 7.** (a) Photograph of the whole tactile sensor matrix touched by a human finger underneath a homemade reservoir. (b-c) Measured time-resolved voltage outputs of one device by finger tapping in water (b) and air (c). (d) Measured time-resolved voltage curve of one pixel result from contacts with different materials, i.e., Al, polymer, and human skin.

potential toward practical applications for low power wearable electronics, artificial skins, *etc.*

## EXPERIMENTAL SECTION

**Fabrication of the Waterproof Self-Powered Tactile Sensing Array.** To fabricate the Si mold for the PDMS film, a 4 in. (100) Si wafer was first covered by a wet thermal grown SiO<sub>2</sub> layer with 1 μm thickness as a hard mask and patterned by photolithography. After dry etching of the SiO<sub>2</sub> hard mask, the wafer was etched anisotropically using a wet etching recipe of 25% tetramethylammonium hydroxide (TMAH) at 80 °C, resulting in a trench network as the template for PDMS walls. By repeating the above processes with a different pattern on the same wafer to form inverted pyramids, the Si wafer surface was shaped with two different structures for PDMS walls and pyramids, respectively. After having been cleaned with acetone and isopropyl alcohol, the Si template was silanized by trichloro(1H,1H,2H,2H-perfluorooctyl) silane (Sigma-Aldrich) vapor to reduce the adhesion force between the PDMS film and the Si wafer. Thereafter, the PDMS elastomer mixture (Sylgard 184, Dow Corning) with a 10:1 ratio (w/w) of the base and the curing agent was stirred, degassed, and spin-coated at 450 rpm for 5 min on the Si template. After 1 h curing at 100 °C, the PDMS film with proper structures was peeled off carefully. To fabricate bottom ITO electrodes, a piece of ITO-coated PET film (Sigma-Aldrich) was cut by a 100 μm CO<sub>2</sub> laser beam into a 100-pixel electrode array with connections interfacing with a custom designed PCB. Then the PET film was placed under the PDMS film with the bottom electrode pixels well aligned with the PDMS pyramid arrays. Then another continuous clean ITO-coated PET film was covered on the top of the PDMS film as the common ground for all the sensing devices, and the whole device was sealed by ordinary adhesive tape. Silver paste and copper wires were used to connect ITO pads of the tactile sensors to the PCB copper pads. The dimension of each touch

pixel is 4 mm × 4 mm, and the total size of the whole sensor array is around 5 cm × 5 cm × 500 μm.

**Measurement of the Fabricated Devices.** The characterization of the tactile sensor array was conducted by a homemade testing system. The tactile sensor array was mounted on a customized PCB with a loading resistance to connect with the measurement circuit. The output signals of the sensors were selected by utilizing a multiplexer (National Instruments PXI-2530B High-Density Multiplexer) in real time and recorded by using an electrometer (Keithley 6514 System Electrometer), and simultaneously the mechanical loading was measured by a force sensor under the sample. The waterproof testing of the tactile sensor array was conducted in a homemade reservoir made of a waterproof tape (3M 2228-1 × 10FT Self Amalgamating Tape).

## ASSOCIATED CONTENT

### Supporting Information

The Supporting Information is available free of charge on the ACS Publications website at DOI: 10.1021/acsnano.6b03042.

Movie 1, the repeating test of multiple touches in real-time (AVI)

Movie 2, the time-resolved touch sensing demonstration under water (AVI)

Movie 3, its control group in air (AVI)

Movie 4, the real-time touch sensing test with different materials (AVI)

## AUTHOR INFORMATION

### Corresponding Authors

\*E-mail: zhangty@shu.edu.cn.

\*E-mail: eezfan@ust.hk.

## Notes

The authors declare no competing financial interest.

## ACKNOWLEDGMENTS

This work was supported by General Research Fund (No. 622312 and No. 612113) from Hong Kong Research Grants Council and Hong Kong Innovation and Technology Fund (ITS/117/13, ITS/362/14FP) from the Innovation and Technology Commission. T.Y.Z. is grateful for the financial support by the research grants (No.14DZ2261200 and No. 15DZ2260300) from the Science and Technology Commission of Shanghai Municipality.

## REFERENCES

- (1) Gao, W.; Emaminejad, S.; Nyein, H. Y.; Challa, S.; Chen, K.; Peck, A.; Fahad, H. M.; Ota, H.; Shiraki, H.; Kiriya, D.; Lien, D. H.; Brooks, G. A.; Davis, R. W.; Javey, A. Fully Integrated Wearable Sensor Arrays for Multiplexed *In Situ* Perspiration Analysis. *Nature* **2016**, *529*, 509–514.
- (2) Hu, K.; Xiong, R.; Guo, H.; Ma, R.; Zhang, S.; Wang, Z. L.; Tsukruk, V. V. Self-Powered Electronic Skin with Biotactile Selectivity. *Adv. Mater.* **2016**, *28*, 3549.
- (3) Kaltenbrunner, M.; Sekitani, T.; Reeder, J.; Yokota, T.; Kuribara, K.; Tokuhara, T.; Drack, M.; Schwodiauer, R.; Graz, I.; Bauer-Gogonea, S.; Bauer, S.; Someya, T. An Ultra-Lightweight Design for Imperceptible Plastic Electronics. *Nature* **2013**, *499*, 458–463.
- (4) Lipomi, D. J.; Vosgueritchian, M.; Tee, B. C.; Hellstrom, S. L.; Lee, J. A.; Fox, C. H.; Bao, Z. Skin-Like Pressure and Strain Sensors Based on Transparent Elastic Films of Carbon Nanotubes. *Nat. Nanotechnol.* **2011**, *6*, 788–792.
- (5) Someya, T.; Sekitani, T.; Iba, S.; Kato, Y.; Kawaguchi, H.; Sakurai, T. A Large-Area, Flexible Pressure Sensor Matrix with Organic Field-Effect Transistors for Artificial Skin Applications. *Proc. Natl. Acad. Sci. U. S. A.* **2004**, *101*, 9966–9970.
- (6) Takei, K.; Takahashi, T.; Ho, J. C.; Ko, H.; Gillies, A. G.; Leu, P. W.; Fearing, R. S.; Javey, A. Nanowire Active-Matrix Circuitry for Low-Voltage Macroscale Artificial Skin. *Nat. Mater.* **2010**, *9*, 821–826.
- (7) Wu, W.; Wen, X.; Wang, Z. L. Taxel-Addressable Matrix of Vertical-Nanowire Piezotronic Transistors for Active/Adaptive Tactile Imaging. *Science* **2013**, *340*, 952–957.
- (8) Xu, S.; Zhang, Y.; Jia, L.; Mathewson, K. E.; Jang, K. I.; Kim, J.; Fu, H.; Huang, X.; Chava, P.; Wang, R.; Bhole, S.; Wang, L.; Na, Y. J.; Guan, Y.; Flavin, M.; Han, Z.; Huang, Y.; Rogers, J. A. Soft Microfluidic Assemblies of Sensors, Circuits, and Radios for the Skin. *Science* **2014**, *344*, 70–74.
- (9) Chen, J.; Zhu, G.; Yang, J.; Jing, Q.; Bai, P.; Yang, W.; Qi, X.; Su, Y.; Wang, Z. L. Personalized Keystroke Dynamics for Self-Powered Human–Machine Interfacing. *ACS Nano* **2015**, *9*, 105–116.
- (10) Dhakar, L.; Pitchappa, P.; Tay, F. E. H.; Lee, C. An Intelligent Skin Based Self-Powered Finger Motion Sensor Integrated with Triboelectric Nanogenerator. *Nano Energy* **2016**, *19*, 532–540.
- (11) Yang, W.; Chen, J.; Wen, X.; Jing, Q.; Yang, J.; Su, Y.; Zhu, G.; Wu, W.; Wang, Z. L. Triboelectrification Based Motion Sensor for Human-Machine Interfacing. *ACS Appl. Mater. Interfaces* **2014**, *6*, 7479–7484.
- (12) Yang, Y.; Zhang, H. L.; Lin, Z. H.; Zhou, Y. S.; Jing, Q. S.; Su, Y. J.; Yang, J.; Chen, J.; Hu, C. G.; Wang, Z. L. Human Skin Based Triboelectric Nanogenerators for Harvesting Biomechanical Energy and as Self-Powered Active Tactile Sensor System. *ACS Nano* **2013**, *7*, 9213–9222.
- (13) Chang, C.; Tran, V. H.; Wang, J.; Fuh, Y. K.; Lin, L. Direct-Write Piezoelectric Polymeric Nanogenerator with High Energy Conversion Efficiency. *Nano Lett.* **2010**, *10*, 726–731.
- (14) Chen, X.; Xu, S.; Yao, N.; Shi, Y. 1.6 V Nanogenerator for Mechanical Energy Harvesting Using PZT Nanofibers. *Nano Lett.* **2010**, *10*, 2133–2137.
- (15) Xie, Y.; Wang, S.; Lin, L.; Jing, Q.; Lin, Z. H.; Niu, S.; Wu, Z.; Wang, Z. L. Rotary Triboelectric Nanogenerator Based on a Hybridized Mechanism for Harvesting Wind Energy. *ACS Nano* **2013**, *7*, 7119–7125.
- (16) Zhang, L.; Zhang, B.; Chen, J.; Jin, L.; Deng, W.; Tang, J.; Zhang, H.; Pan, H.; Zhu, M.; Yang, W.; Wang, Z. L. Lawn Structured Triboelectric Nanogenerators for Scavenging Sweeping Wind Energy on Rooftops. *Adv. Mater.* **2016**, *28*, 1650–1656.
- (17) Zheng, L.; Cheng, G.; Chen, J.; Lin, L.; Wang, J.; Liu, Y.; Li, H.; Wang, Z. L. A Hybridized Power Panel to Simultaneously Generate Electricity from Sunlight, Raindrops, and Wind around the Clock. *Adv. Energy Mater.* **2015**, *5*, 1501152.
- (18) Zheng, Q.; Shi, B.; Fan, F.; Wang, X.; Yan, L.; Yuan, W.; Wang, S.; Liu, H.; Li, Z.; Wang, Z. L. *In Vivo* Powering of Pacemaker by Breathing-Driven Implanted Triboelectric Nanogenerator. *Adv. Mater.* **2014**, *26*, 5851–5856.
- (19) Zhu, G.; Lin, Z. H.; Jing, Q.; Bai, P.; Pan, C.; Yang, Y.; Zhou, Y.; Wang, Z. L. Toward Large-Scale Energy Harvesting by a Nanoparticle-Enhanced Triboelectric Nanogenerator. *Nano Lett.* **2013**, *13*, 847–853.
- (20) Zhu, G.; Su, Y.; Bai, P.; Chen, J.; Jing, Q.; Yang, W.; Wang, Z. L. Harvesting Water Wave Energy by Asymmetric Screening of Electrostatic Charges on a Nanostructured Hydrophobic Thin-Film Surface. *ACS Nano* **2014**, *8*, 6031–6037.
- (21) Zhu, G.; Yang, W. Q.; Zhang, T.; Jing, Q.; Chen, J.; Zhou, Y. S.; Bai, P.; Wang, Z. L. Self-Powered, Ultrasensitive, Flexible Tactile Sensors Based on Contact Electrification. *Nano Lett.* **2014**, *14*, 3208–13.
- (22) Chen, J.; Yang, J.; Li, Z.; Fan, X.; Zi, Y.; Jing, Q.; Guo, H.; Wen, Z.; Pradel, K. C.; Niu, S.; Wang, Z. L. Networks of Triboelectric Nanogenerators for Harvesting Water Wave Energy: a Potential Approach Toward Blue Energy. *ACS Nano* **2015**, *9*, 3324–3331.
- (23) Su, Y.; Wen, X.; Zhu, G.; Yang, J.; Chen, J.; Bai, P.; Wu, Z.; Jiang, Y.; Lin, W.; Wang, Z. Hybrid Triboelectric Nanogenerator for Harvesting Water Wave Energy and as a Self-Powered Distress Signal Emitter. *Nano Energy* **2014**, *9*, 186–195.
- (24) Fan, F. R.; Lin, L.; Zhu, G.; Wu, W.; Zhang, R.; Wang, Z. L. Transparent Triboelectric Nanogenerators and Self-Powered Pressure Sensors Based on Micropatterned Plastic Films. *Nano Lett.* **2012**, *12*, 3109–3114.
- (25) Tang, W.; Meng, B.; Zhang, H. X. Investigation of Power Generation Based on Stacked Triboelectric Nanogenerator. *Nano Energy* **2013**, *2*, 1164–1171.
- (26) Wang, S.; Lin, L.; Wang, Z. L. Nanoscale Triboelectric-Effect-Enabled Energy Conversion for Sustainably Powering Portable Electronics. *Nano Lett.* **2012**, *12*, 6339–6346.
- (27) Zhang, X. S.; Han, M. D.; Wang, R. X.; Zhu, F. Y.; Li, Z. H.; Wang, W.; Zhang, H. X. Frequency-Multiplication High-Output Triboelectric Nanogenerator for Sustainably Powering Biomedical Microsystems. *Nano Lett.* **2013**, *13*, 1168–1172.
- (28) Ko, Y. H.; Lee, S. H.; Leem, J. W.; Yu, J. S. High Transparency and Triboelectric Charge Generation Properties of Nano-Patterned PDMS. *RSC Adv.* **2014**, *4*, 10216–10220.